Assessment of 10CrMo9-10 Power Engineering Steel Degradation State by Using Small Punch Test

Kamil Majchrowicz [1,*], Barbara Romelczyk-Baishya [1], Monika Wieczorek-Czarnocka [1], Szymon Marciniak [1], Milena Mras [1], Dominik Kukla [2], Mateusz Kopec [2,3] and Zbigniew Pakieła [1]

1   Faculty of Materials Science and Engineering, Warsaw University of Technology, Wołoska 141, 02-507 Warsaw, Poland; barbara.romelczyk-baishya@pw.edu.pl (B.R.-B.); monika.wieczorek-czarnocka@pw.edu.pl (M.W.-C.); szymon.marciniak@pw.edu.pl (S.M.); milena.mras.stud@pw.edu.pl (M.M.); zbigniew.pakiela@pw.edu.pl (Z.P.)
2   Institute of Fundamental Technological Research, Polish Academy of Sciences, Pawińskiego 5b, 02-106 Warsaw, Poland; dkukla@ippt.pan.pl (D.K.); mkopec@ippt.pan.pl (M.K.)
3   College of Science and Engineering, University of Derby, Markeaton Street, Derby DE22 3AW, UK
*   Correspondence: kamil.majchrowicz@pw.edu.pl

Abstract

Degradation of power engineering steel structures requires constant monitoring of their mechanical properties to estimate remaining service life. Therefore, the current study aimed to develop a methodology that will enable for accurate determination of changes in mechanical properties of 10CrMo9-10 steel after long-term exploitation involving the Small Punch Test (SPT). Firstly, the as-received 10CrMo9-10 steel was annealed at 770 °C for different periods (1.5, 6 and 24 h) to deteriorate its strength to a level similar to its exploited counterpart. Then, mechanical properties were characterized by uniaxial tensile tests and the SPT method using miniaturized discs with a diameter of 8 mm and a thickness of 0.5 mm as recommended by the EN 10371:2021 standard. It allowed to determine a formula correlating the SPT results (i.e., elastic–plastic transition force and maximum force) with the yield and ultimate tensile strength. The $\beta_{Rp0.2}$ and β_{Rm} correlation factors were equal to 0.437 and 0.255, respectively. Finally, the exploited 10CrMo9-10 steel was tested by the SPT method. Based on the SPT results, the values of $R_{p0.2}$ = 236 ± 27 MPa and R_m = 459 ± 17 MPa were estimated, which were close to those assessed during the uniaxial tensile tests ($R_{p0.2}$ = 218 ± 3 MPa and R_m = 454 ± 4 MPa). It was shown that the application of such a relatively simple method is a promising way for determining the changes in mechanical properties of structural steels after long-term service at elevated temperature.

Keywords: 10CrMo9-10 steel; small punch test; mechanical properties; degradation

1. Introduction

10CrMo9-10 (also known as 10H2M or 1.7380) is a chrome-molybdenum-manganese, creep-resistant steel which is widely used in thermal power plants due to its ability to withstand long-term service under elevated temperature and high pressure [1–3]. Typically, such Cr-Mo-Mn steels are intended for boilers and steam turbine components operating at temperatures up to 580 °C [3,4]. The addition of Cr enhances strength, hardness and corrosion and oxidation resistance. Molybdenum is particularly effective at improving strength and impact toughness, while Mn is a key element for increasing weldability and ductility [5,6]. Moreover, Cr, Mo and Mn significantly enhance hardenability and promote

the formation of uniform and fine microstructures, such as bainitic and martensitic, with numerous carbide precipitates [5,6]. Depending on the applied normalizing and tempering or quenching and tempering parameters, 10CrMo9-10 steel may exhibit a martensitic, bainitic or mixed bainitic–ferritic microstructure [3,7,8]. The microstructure type is controlled by the applied cooling rate, with faster cooling favouring martensite formation [6].

The degradation of structural steels in thermal power plants is related to different damage mechanisms, such as creep damage, high temperature fatigue, thermal ageing and microstructural degradation leading to embrittlement, hydrogen damage, erosion or high temperature corrosion and oxidation [9]. Cr-Mo steels are mainly susceptible to microstructural degradation due to coarsening of carbides or impurity segregation at grain boundaries [10,11]. During long-term exposure at elevated temperature, the microstructure degradation process results in the coarsening of martensite or bainite laths into broader ferrite laths and subsequently into equiaxed ferrite grains. Additionally, the coarsening of M_2X carbides into larger $M_{23}C_6$ and/or M_6C carbides occurs, leading to the formation of an equiaxed ferrite grain structure with the coarse carbides concentrated on the ferrite grain boundaries [1,2,7]. Such microstructure reorganization significantly deteriorates the mechanical properties of 10CrMo9-10 steel components [2,7]. This implies a need for their constant monitoring through a series of non-destructive and destructive tests [1]. The assessment of the current condition of steel is mainly realized by a comparative study of the as-received and exploited materials with standard requirements [12,13]. It mainly covers the characterization of microstructural changes and mechanical properties determined during tensile and Charpy tests [7], or additional fatigue [2,13] and creep tests [14]. This approach typically requires a relatively high volume of tested material and a long time of structure shut down in order to perform a complete evaluation of its current condition.

The small punch test (SPT) is a method that enables the characterization of different mechanical properties of small-scale materials with a limited volume [15,16] or materials extracted from in-service components [17]. During the SPT, a disc-shaped or rectangular miniaturized specimen (having a size of a few millimetres) is deformed through a die using a hemispherical punch. Subsequently, the recorded load–deflection data is adopted for the estimation of the tensile strength, fracture toughness or creep properties [15,18]. A successful estimation of a yield strength ($R_{p0.2}$) and ultimate tensile strength (R_m) [18,19], along with the evaluation of fracture toughness [20–22], ductile-to-brittle transition temperatures [23,24] or creep properties [25,26] has been widely reported in recent years. As a consequence, the European Committee for Standardization has recently approved this method in the EN 10371:2021 standard [27]. According to this standard, a linear correlations of the SPT results with the $R_{p0.2}$ and R_m values were proposed as follows:

$$R_{p0.2} = \beta_{Rp0.2} \cdot \frac{F_e}{h_0{}^2} \tag{1}$$

$$R_m = \beta_{Rm} \cdot \frac{F_m}{(h_0 \cdot u_m)} \tag{2}$$

where h_0 is an initial specimen thickness, F_e is an elastic–plastic transition force in the small punch test, F_m is a maximum force during the test, u_m is a deflection at the maximum force, and $\beta_{Rp0.2}$ and β_{Rm} are correlation factors for estimation of $R_{p0.2}$ and R_m, respectively.

Kumar et al. [28] reported the β_{Rm} value of 0.281 based on the SPT results of 20Mn-MoNi55, CrMoV and SS304LN steels using miniaturized discs with a diameter of 3 mm and a thickness of 0.25 mm punched through a die with a diameter of 1.5 mm. In turn, Garcia et al. [29] used rectangular 10 mm × 10 mm blanks with a thickness of 0.5 mm to investigate a wide range of steels with a different strength, i.e., two experimental grades of Eurofer steel, four grades of vanadium-modified 2.25Cr1Mo steels, automobile dual

phase steels, AISI 304 and D2205 stainless steels, and general structural steels such as S460, API X70 and AR. The authors obtained the $\beta_{Rp0.2}$ and β_{Rm} factors of 0.442 and 0.277, respectively, showing that these coefficients are less sensitive to the tested material. Similar findings were reported by Altstadt et al. [30] who used disc-shaped specimens having a diameter of 8 mm and a thickness of 0.5 mm made of P91, P92, Eurofer97, 22NiMoCr37 and 15Kh2MFA steels. The β_{Rm} factor varied from 0.254 to 0.299 depending on the tested material, with the average value for all materials equal to 0.278. It was concluded that the SPT correlation coefficients are more dependent on the geometry parameters of the testing setup, i.e., the specimen size and thickness, the radius of the punch, a receiving hole diameter or a chamfer size and shape. It has been clearly shown by Altstadt et al. [31] for the T91 steel that the $\beta_{Rp0.2}$ and β_{Rm} factors may differ from 0.42 to 0.63 and 0.19 to 0.26, respectively, depending on the used SPT setup.

Since the SPT proved its efficiency in steel testing, the current study aimed to develop a methodology for determining changes in the mechanical properties of 10CrMo9-10 steel after long-term exploitation (280,000 h) at elevated temperature and internal pressure (540 °C and 2.9 MPa) using the SPT method. Since such steel is one of the most popular steels in the power engineering sector in Poland [32] or Czech Republic [33], the assessment of its mechanical performance after prolonged service is of great importance. In addition, to the best of the authors' knowledge, no literature references provide the exact correlation factors for estimation of $R_{p0.2}$ and R_m from the SPT results according the current EN 10371:2021 standard. So far, Andres et al. [33] and Dymacek et al. [34] have focused on the creep properties of the exploited 10CrMo9-10 steel, while Kaliciak et al. [35] did not present any correlation formulas for recalculating the SPT results.

2. Materials and Methods

The chemical composition of the investigated 10CrMo9-10 steel in the as-received and exploited state was presented in Table 1 with respect to the EN 10028-2:2017 standard requirements [36]. The exploited material was a part of a pipe having a diameter of about 500 mm and a wall thickness of 20 mm, which operated for 280,000 h at the internal pressure of 2.9 MPa under a temperature of 540 °C. The as-received 10CrMo9-10 steel was cut into cylindrical slabs with a diameter of 60 mm and a thickness of 25 mm and annealed at 770 °C for 1.5, 6 and 24 h to obtain several conditions with gradually deteriorated mechanical properties to the final level similar to its exploited counterpart. Furthermore, such different material states will allow to estimate the linear correlations of the SPT results with the standard tensile parameters (i.e., $R_{p0.2}$ and R_m). The annealing temperature was established based on the dilatometric measurements performed on a representative sample in the form of a rod with a diameter of 3 mm and a length of 10 mm using a TA Instruments DIL805L (TA Instruments, New Castle, DE, USA) dilatometer at a heating rate of 0.3 °C/min.

Table 1. Chemical composition of as-received and exploited 10CrMo9-10 steel.

Material	C	Si	Mn	Cr	Mo	Fe
As-received	0.12	0.37	0.42	2.00	0.90	Balanced
Exploited	0.16	0.44	0.61	2.51	0.98	Balanced
EN 10028-2	0.08–0.14	≤0.50	0.40–0.80	2.00–2.50	0.90–1.10	Balanced

The microstructure of 10CrMo9-10 steel was characterized by a Zeiss Axio Observer (Carl Zeiss Microscopy GmbH, Jena, Germany) microscope. Sections for microscopic observations were ground, polished and etched with a solution of 10% nital. The microstructure was quantified in terms of a mean grain boundary density (S_V), carbide precipitate density (N_A) and a fraction of equiaxed ferrite grains (V_V) using an ImageJ software (v1.53k). A line-intercept method was used for the grain boundary density measurement. The Vickers

hardness measurements (at least 10 indentations per sample) were conducted at a load of 5 kg using an Innovatest Falcon 500 (Innovatest Europe BV, Maastricht, The Netherlands) hardness tester.

The tensile properties of the as-received state were assessed according to the ISO 6892-1 standard [37] using standard flat samples with a gauge length of 25 mm and a cross section of 3.8 mm × 5.1 mm as well as miniaturized flat samples with the different gauge length of 8, 4 and 2 mm and proportional cross sections (as shown in Figure 1a). Such tests aimed to find an optimal sample geometry to minimize the specimen size which can be directly extracted from in-service components without a need of repair after material removal. A scoop cutter sampling technique can be used for such purposes [27,38]. It is a unique hemispherical shell cutter capable of removing a disc-shaped material volume (typically with a diameter of approximately 40 mm and a thickness of 4 mm) without mechanical distortion or thermal degradation of the component [27,38]. All other states were examined using miniaturized test specimens with a gauge length of 8 mm showing the same results as the standard ones. Uniaxial tensile tests of standard specimens were performed using an MTS 810 (MTS Systems Corp., Eden Prairie, MN, USA) servo-hydraulic testing machine equipped with a 100 kN load cell and an MTS 632.24F-50 extensometer. The miniaturized test specimens were tested using a Zwick Roell Z005 (Zwick GmbH & Co. KG, Ulm, Germany) testing machine with a 5 kN loading capacity and a digital image correlation (DIC) system for strain measurements (described in more detail in [39,40]). All tensile tests were conducted at the initial strain rate of 10^{-3} s^{-1}. Each material state was represented by at least five samples cut by the electric discharge machining (EDM) method along the rod or pipe axis. The measurement uncertainties were calculated according to Annex J from the ISO 6892-1 standard as the combined uncertainty of the standard deviations and the accuracy of the measuring equipment, i.e., the load cell ($\pm$0.5%), extensometer ($\pm$0.5%) or DIC strain measurement system ($\pm$1%), gauge length, and cross section measurements ($\pm$1%).
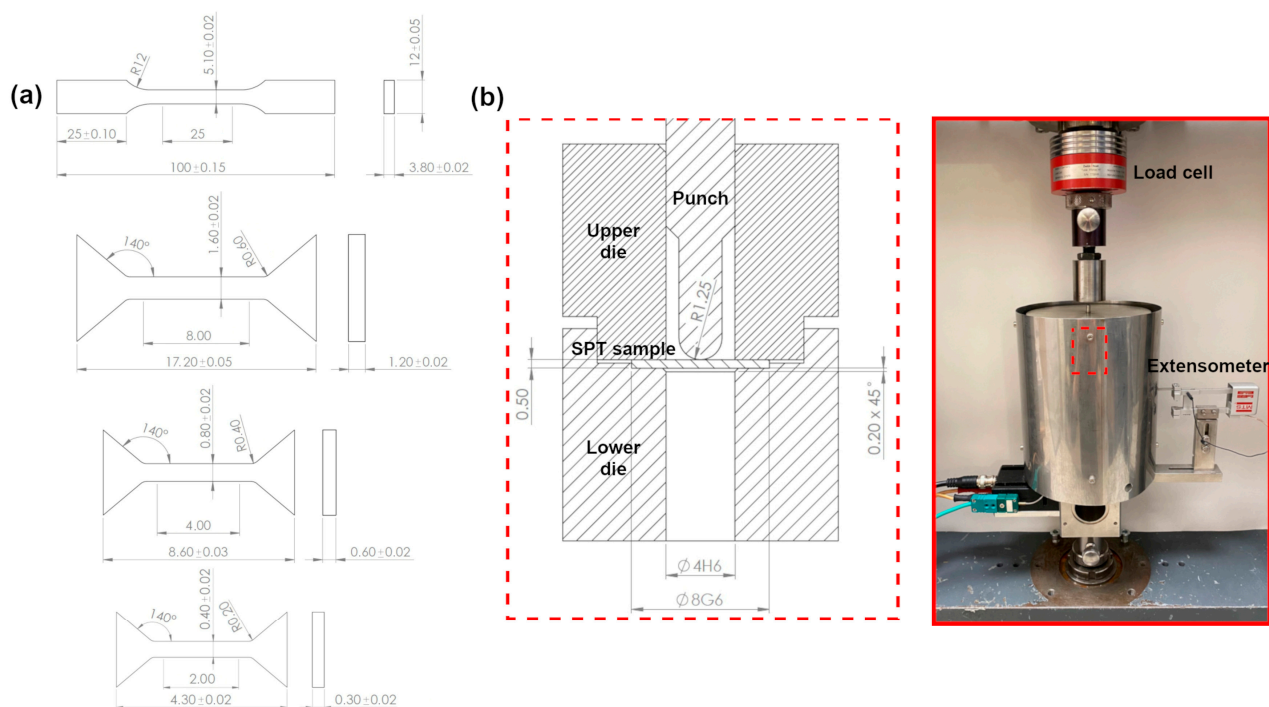

Figure 1. (**a**) Technical drawings of flat standard and miniaturized tensile samples and (**b**) schematic and general view of the SPT experimental setup.

The experimental SPT setup consisted of a lower die with a receiving hole diameter of 4 mm and a chamfer of 0.2 mm × 45° and a spherically ended punch having a radius of 1.25 mm as recommended by the EN 10371:2021 standard [27] (Figure 1b). The deflection was measured by an MTS 634.12F-25 extensometer (MTS Systems, Berlin, Germany) attached to the lower surface of the sample. Before the tests, the disc-shaped SPT samples with a diameter of 8 mm were ground using 1200-grit SiC paper to obtain the required thickness of 0.5 ± 0.005 mm. The SPTs were conducted on a Zwick Roell Z005 (Zwick GmbH & Co. KG, Ulm, Germany) testing machine at a crosshead speed of 0.5 mm/min. At least five SPT samples were tested from each material state. The measurement uncertainties of the load and deflection were estimated based on the standard deviations and the equipment errors (i.e., the accuracy of load cell ± 0.5% and extensometer ± 0.5%).

3. Results and Discussion

3.1. Heat Treatment

The dilatometric measurements were firstly performed for the as-received 10CrMo9-10 steel in order to determine the maximum heat treatment temperature to avoid austenitic transformation. The measured length change as a function of temperature is presented in Figure 2a. The calculated onset temperature of austenitic transformation was around 781 °C, which is very close to the temperature reported by Ławrynowicz [3], i.e., 780 °C. Thus, the as-received 10CrMo9-10 was annealed at 770 °C for a specified time of 1.5, 6 and 24 h. The changes in the Vickers hardness of the annealed samples are shown in Figure 2b. Hardness gradually decreased from 174 ± 2 HV5 for the as-received state to the value of 131 ± 2 HV5 after 24 h of annealing, which was practically the same as the hardness of the exploited 10CrMo9-10 steel (i.e., 132 ± 3 HV5).
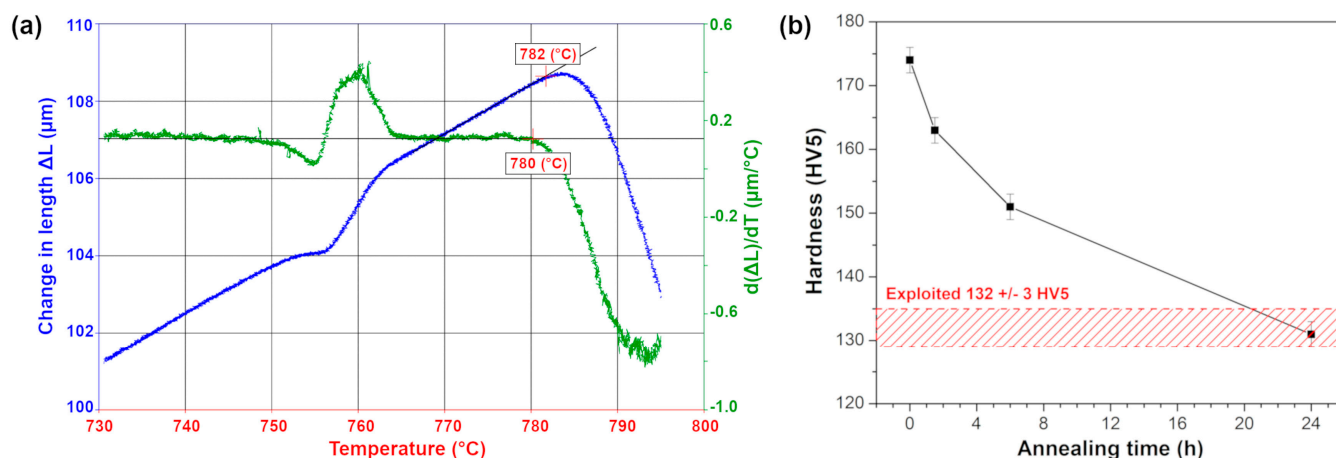

Figure 2. (**a**) Dilatometric curve of as-received 10CrMo9-10 steel and (**b**) Vickers hardness changes as a function of annealing time at 770 °C.

3.2. Microstructure

Figure 3a–e presents the microstructure of the 10CrMo9-10 steel in the as-received, annealed and exploited states. The as-received 10CrMo9-10 steel exhibited a fully bainitic microstructure with carbides located at grain boundaries and inside grains, which is commonly observed in this steel grade, as reported by Gwóździk et al. [7] and Wang et al. [8]. During annealing at 770 °C, the bainite laths transformed into broader ones and subsequently into equiaxed ferrite grains, while the observed carbides coarsened and segregated on the ferrite grain boundaries, as presented for the 10CrMo9-10 steel after annealing for 24 h. The calculated grain boundaries density S_V and carbide precipitates density N_A gradually decreased for longer annealing periods, as shown in Figure 3f, whereas the

fraction of equiaxed ferrite grains increased and became a dominant constituent after 24 h of annealing. In turn, the microstructure of the exploited state consisted of a mixture of degraded bainite and a lower content of ferrite grains with numerous carbides concentrated at grain boundaries. Similar microstructural changes during long-term exposure at elevated temperature of 10CrMo9-10 steel were reported earlier by Brodecki et al. [2], Gwoździk et al. [7] or Kopec et al. [41], which resulted in a significant deterioration of its mechanical performance [2,7,41].
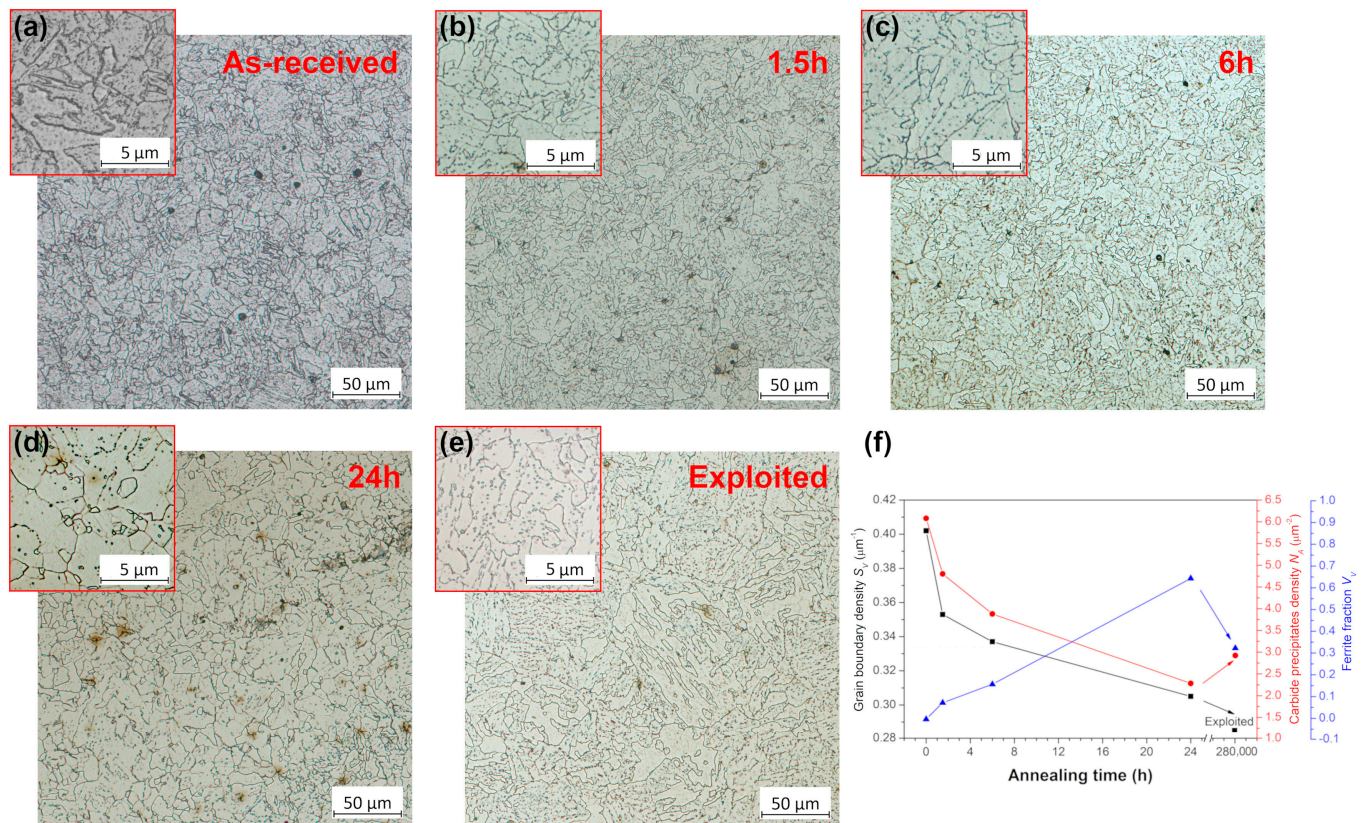

Figure 3. Microstructure of (**a**) as-received, (**b**–**d**) annealed and (**e**) exploited 10CrMo9-10 steel; (**f**) grain boundary–carbide precipitates–ferrite fraction relation as a function of annealing time.

3.3. Tensile Properties

The effect of specimen geometry on the tensile properties of the as-received 10CrMo9-10 steel is presented in Figure 4a and Table 2. The following mechanical parameters were achieved for the as-received 10CrMo9-10 steel tested by the standard size samples: the 0.2% offset yield strength $R_{p0.2}$ = 407 ± 11 MPa, the ultimate tensile strength R_m = 538 ± 6 MPa, the uniform elongation A_u = 11.7 ± 0.2% and the elongation at break A = 32.1 ± 1.9%. The miniaturized samples with the gauge length of 8 mm showed very similar mechanical properties to the standard ones, while all smaller specimens differed significantly. As the specimen size decreased, the measured strength and elongation values were diminished compared to the standard samples. Such a tendency is consistent with the findings of Molak et al. [39] or Kals et al. [42], and it is related to an increasing fraction of surface grains in smaller samples, which do not strengthen the material so effectively as internal grains. Thus, all other conditions of the 10CrMo9-10 steel were examined using miniaturized test specimens with a gauge length of 8 mm, showing the same results as the standard ones.
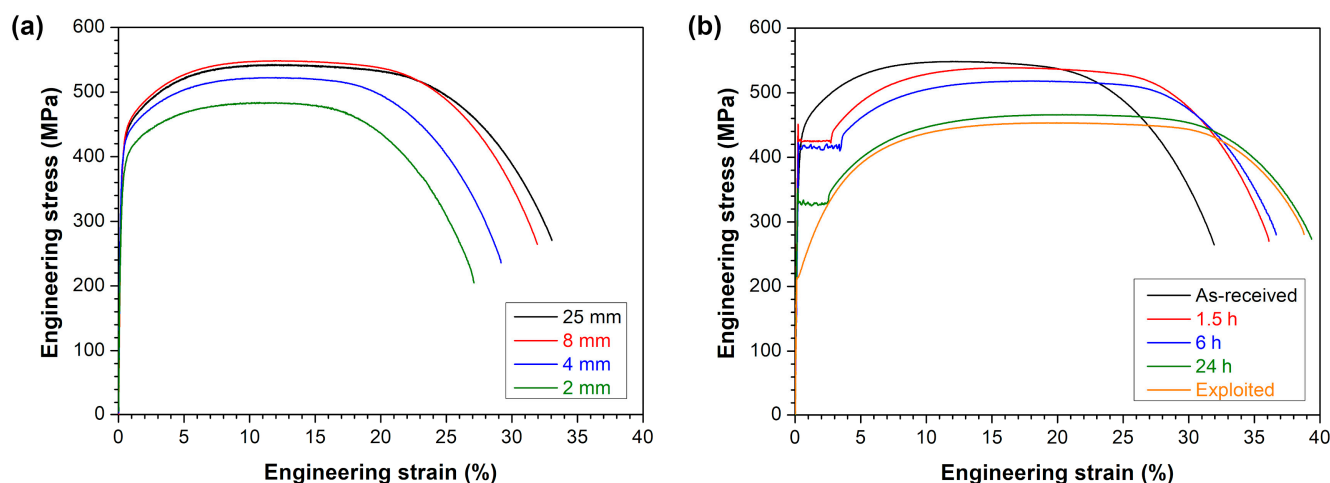
Figure 4. Representative stress–strain curves of 10CrMo9-10 steel in: (**a**) as-received state for different specimen size, (**b**) as-received, annealed and exploited conditions.

Table 2. Mechanical properties of as-received, annealed and exploited 10CrMo9-10 steel ($R_{p0.2}$—0.2% offset yield strength, R_{eH}—upper yield strength, R_{eL}—lower yield strength, R_m—ultimate tensile strength, A_u—uniform elongation, A—elongation at break, F_e—elastic–plastic transition force in small punch test, F_m—maximum force during small punch test, u_m—deflection at maximum force).

Material	$R_{p0.2}$ or R_{eH}/R_{eL} (MPa)	R_m (MPa)	A_u (%)	A (%)	F_e (N)	F_m (N)	u_m (mm)
As-received (25 mm)	407 ± 11	538 ± 6	11.7 ± 0.2	32.1 ± 1.9			
As-received (8 mm)	421 ± 6	544 ± 7	12.0 ± 0.1	31.7 ± 0.8	234 ± 13	1607 ± 28	1.53 ± 0.02
As-received (4 mm)	398 ± 8	520 ± 7	11.8 ± 0.3	29.3 ± 1.3			
As-received (2 mm)	375 ± 9	484 ± 6	11.0 ± 0.5	27.8 ± 2.0			
Annealed 1.5 h	$437 \pm 14/422 \pm 5$	539 ± 4	16.1 ± 0.3	34.3 ± 1.5	236 ± 2	1634 ± 25	1.55 ± 0.01
Annealed 6 h	$430 \pm 10/410 \pm 7$	517 ± 4	17.4 ± 0.4	34.9 ± 1.3	234 ± 8	1599 ± 13	1.58 ± 0.01
Annealed 24 h	$344 \pm 7/328 \pm 4$	467 ± 4	20.3 ± 0.5	37.3 ± 2.1	189 ± 5	1519 ± 25	1.60 ± 0.01
Exploited	218 ± 3	454 ± 4	19.1 ± 0.3	36.6 ± 1.3	135 ± 16	1464 ± 47	1.62 ± 0.02

The comparison of representative stress–strain curves of the as-received, annealed and exploited 10CrMo9-10 steel is shown in Figure 4b, and the calculated mechanical parameters are summarized in Table 2. All annealed conditions exhibited an upper (R_{eH}) and lower (R_{eL}) yield strength, whereas the 0.2% offset yield strength ($R_{p0.2}$) values were estimated for the as-received and exploited states. In general, the strength values decreased gradually with the prolongation of the annealing time, whereas the elongation values showed the opposite trend. The 10CrMo9-10 steel annealed for the longest period of 24 h exhibited R_m of 467 ± 4 MPa and A of $37.3 \pm 2.1\%$ comparable to the exploited state ($R_m = 454 \pm 4$ MPa, $A = 36.6 \pm 1.3\%$), which is consistent with the hardness measurements presented in Figure 2b. At the same time, the exploited condition showed much lower $R_{p0.2} = 218 \pm 3$ MPa than the annealed state after 24 h ($R_{eH} = 344 \pm 7$ MPa and $R_{eL} = 328 \pm 4$ MPa).

3.4. SPT Results

In order to determine the linear correlations of the SPT results with the uniaxial tensile tests, the as-received, annealed and exploited 10CrMo9-10 steel was tested by using the SPT method. The representative load–deflection curves are shown in Figure 5, while Table 2 presents the average values of the elastic–plastic transition force (F_e), maximum force (F_m) and deflection at maximum force (u_m). Four deformation stages, typically observed during SPT of a ductile material, can be distinguished in the obtained load–deflection curves, i.e., (I) elastic bending up to F_e value, (II) plastic bending and (III) membrane stretching until reaching F_m value and (IV) final plastic instability regime [20,43]. The average F_m and u_m

for the as-received state was 1607 ± 28 N and 1.53 ± 0.02 mm. The annealing treatment for 1.5 h resulted in a slight increase in the F_m value (1634 ± 25 N), but further exposition at 770 °C caused a gradual decrease in the maximum force to 1519 ± 25 N after 24 h. In turn, the deflection at maximum force was constantly increased due to the longer annealing treatment (as marked by dotted lines in Figure 5a). It is worth to mention that the changes in F_m and u_m values exhibited the same tendencies as the R_m and A_u during tensile tests. This implies that F_m and u_m values are sensitive to the observed microstructural changes in the same way as the R_m and A_u. The gradual reduction in F_m value and strength of the 10CrMo9-10 steel after longer annealing periods resulted from the gradually decreased grain boundary density S_V and carbide precipitates density N_A (as shown in Figure 3). In turn, the higher content of equiaxed ferrite grains V_V contributed to more uniform deformation and higher u_m and A_u values representing material ductility.
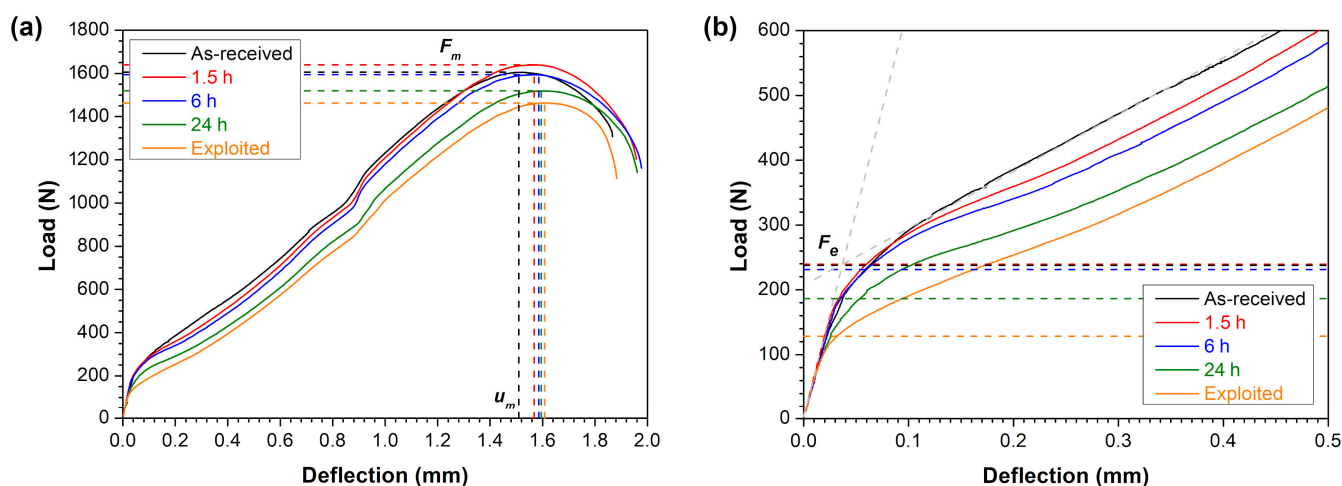

Figure 5. Representative load–deflection curves from SPTs of 10CrMo9-10 steel in as-received, annealed and exploited conditions: (**a**) overall view, (**b**) close-up of elastic bending regime.

The close-up of the elastic bending regime presented in Figure 5b clearly shows that the transition forces F_e for the as-received and annealed states for 1.5 and 6 h were very similar (in the range of 234–236 N), whereas they were drastically reduced for SPT specimens after annealing for 24 h (F_e = 189 ± 5 N) and the exploitation period (F_e = 135 ± 16 N). Such differences in the F_e value are consistent with the tensile results, especially when the R_{eL} values for the annealed conditions are considered, as recommended in the EN 10371:2021 standard. The R_{eL} values for the annealed conditions gradually decreased from 422 ± 5 to 410 ± 7 and 328 ± 4 MPa after 1.5, 6 and 24 h at 770 °C, respectively, while the F_e values were 236 ± 2, 234 ± 8 and 189 ± 5 N, respectively. In turn, the exploited condition clearly showed the lowest values of F_e = 135 ± 16 N and $R_{p0.2}$ = 218 ± 3 MPa. Such differences in the F_e and R_{eL} (or $R_{p0.2}$) values can be linked to the gradually decreased grain boundary density S_V, which contributed to less strengthening according to the well-known Hall–Petch relation [44,45].

Figure 6a presents the correlation function between $R_{p0.2}$ (or R_{eL}) from the uniaxial tensile test and F_e/h_0^2 from the SPTs according to the Formula (1). The correlation factor $\beta_{Rp0.2}$ was equal to 0.437. In turn, the correlation function between R_m and $F_m/(h_0 \, u_m)$ according to the Formula (2) is presented in Figure 6b. The correlation factor β_{Rm} was equal to 0.255. It should be mentioned that both calculated factors are similar to values reported in the literature. Table 3 summarizes the correlation factors with the geometry parameters of the used SPT setups. It has already been shown that the SPT correlation coefficients are more dependent on the SPT setup [31] rather than the investigated material [28–30].

Alstadt et al. [31] noticed for the T91 steel that the $\beta_{Rp0.2}$ and β_{Rm} factors may significantly differ from 0.42 to 0.63 and 0.19 to 0.26, respectively, depending on the used SPT setup, while the effect of the investigated material is less significant (β_{Rm} = 0.254 ÷ 0.299 for P91, P92, Eurofer97, 22NiMoCr37 or 15Kh2MFA steel [30]). In addition, Garcia et al. [29] pointed out that the influence of specimen size and tested material may also vary depending on the applied method of strength correlation, but the empirical correlation equations used in the current SPT standard effectively minimize such effects. According to the EN 10371:2021 standard [27], for the standard geometry used in the current work (i.e., SPT specimen size Φ 8 mm × 0.5 mm, receiving hole diameter 4 mm, chamfer 0.2 × 45°, punch radius 1.25 mm), the coefficient β_{Rm} should be in the range of $0.19 \leq \beta_{Rm} \leq 0.32$. The data presented in Table 3 also shows that the β_{Rm} value for the standard geometry of the SPT setup is in the range from 0.21 to 0.278. Thus, the β_{Rm} value of 0.255 obtained in the current study lies within the expectations. The estimated $\beta_{Rp0.2}$ coefficient of 0.437 is also consistent with other literature references reporting values in the range of 0.42–0.49.
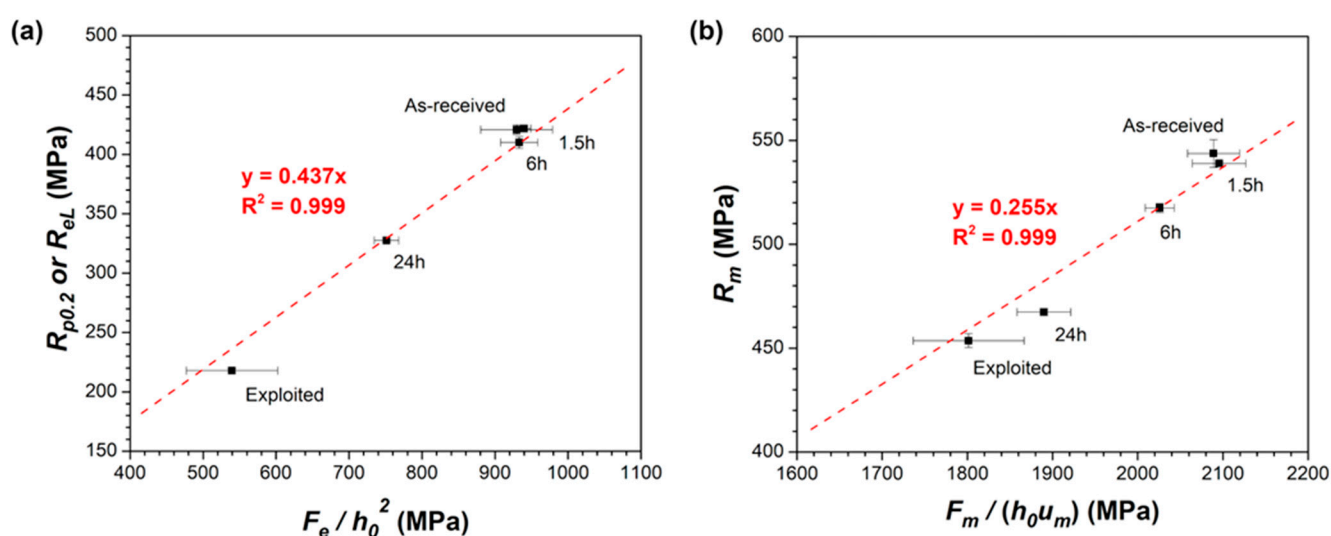

Figure 6. Linear correlations of SPT results with (**a**) yield strength and (**b**) ultimate tensile strength from uniaxial tensile tests.

It should be highlighted that the obtained $\beta_{Rp0.2}$ and β_{Rm} factors allowed the calculation of the $R_{p0.2}$ and R_m of the exploited 10CrMo9-10 steel. Based on the SPT results, the values of $R_{p0.2}$ = 236 ± 27 MPa and R_m = 459 ± 17 MPa were estimated, which were close to $R_{p0.2}$ = 218 ± 3 MPa and R_m = 454 ± 4 MPa assessed in the uniaxial tensile tests. This result proves that the SPT method is a promising way of determining the changes in the mechanical properties of structural steels after long-term service at elevated temperature. Moreover, its predictive capability can be enhanced by incorporating machine learning methods [46,47]. Pan et al. [47] have investigated three different machine learning methods, such as back propagation (BP) neural network, radial basis function (RBF) network and random forest (RF) regression model. The prediction accuracy for pressure vessel steels was in the following order: BP > RBF > RF. The model proposed by Zhong et al. [46] exhibited the mean absolute percentage error in the SPT force prediction in the range of 0.5–2%. Finally, the overall assessment of the degradation state of the 10CrMo9-10 steel components can be improved by additional characterization techniques. The SPT method seems to be effective in the initial screening of mechanical performance (tensile strength, fracture toughness or creep properties), but it should to be supported by the precise characterization of carbide precipitates by transmission electron microscopy, segregation of impurities and possible depletion of alloying elements near grain boundaries by chemical analysis and

Materials **2025**, *18*, 4133

10 of 12

high temperature corrosion and oxidation tests simulating the operational conditions of the 10CrMo9-10 steel.

Table 3. Comparison of correlation factors $\beta_{Rp0.2}$ and β_{Rm} reported in the literature.

$\beta_{Rp0.2}$	β_{Rm}	Specimen Size (mm)	Receiving Hole Diameter (mm)	Chamfer Size or Edge Radius (mm)	Punch Radius (mm)	Materials Tested	Reference
0.437	0.255	$\Phi\,8 \times 0.5$	4	$0.2 \times 45°$	1.25	10CrMo9–10	This work
-	0.281	$\Phi\,3 \times 0.25$	1.5	0.2	0.5	20MnMoNi55, CrMoV steel, SS304LN 2.25Cr1Mo steels,	[28]
0.442	0.277	$10 \times 10 \times 0.5$	4	$0.2 \times 45°$	1.25	dual phase steels, AISI 304, D2205, S460, API X70	[29]
-	0.278	$\Phi\,8 \times 0.5$	4	$0.2 \times 45°$	1.25	P91, P92, Eurofer97, 22NiMoCr37, 15Kh2MFA	[30]
0.63	0.26	$3.5 \times 3.5 \times 0.25$	1.75	0.25	0.5	T91	[31]
0.49	0.26	$10 \times 10 \times 0.5$	4	0.5	1.25	T91	[31]
0.48	0.21	$\Phi\,8 \times 0.5$	4	$0.2 \times 45°$	1.25	T91	[31]
0.42	0.19	$\Phi\,3 \times 0.25$	1.5	0.2	0.5	T91	[31]

4. Conclusions

The aim of this study was to develop a methodology for determining changes in the mechanical properties of 10CrMo9-10 steel using the SPT method, which was later successfully applied to estimate its mechanical performance after long-term exploitation for 280 000 h at 540 °C under pressure of 2.9 MPa. The main conclusions were drawn as follows:

1. The annealing of the as-received 10CrMo9-10 steel (R_m = 544 MPa) at 770 °C for 1.5, 6 and 24 h allowed its strength to gradually decrease to R_m = 539, 517 and 467 MPa, respectively, i.e., to the level similar to the exploited condition (R_m = 454 MPa).
2. The lowered strength resulted from the gradually reduced grain boundary and carbide precipitates densities and the increased fraction of equiaxed ferrite grains after prolonged annealing.
3. The obtained SPT parameters for the as-received, annealed and exploited conditions (i.e., F_e, F_m, u_m) exhibited the same tendencies as the $R_{p0.2}$ (or R_{eL}), R_m and A_u during tensile tests. The following correlation factors were determined $\beta_{Rp0.2}$ = 0.437 and β_{Rm} = 0.255 for the estimation of $R_{p0.2}$ and R_m, respectively.
4. Mechanical parameters of the exploited 10CrMo9-10 estimated based on the SPT results ($R_{p0.2}$ = 236 ± 27 MPa and R_m = 459 ± 17 MPa) were in a good agreement with those assessed during the uniaxial tensile tests (218 ± 3 MPa and R_m = 454 ± 4 MPa).

Institutional Review Board Statement: Not applicable.

Informed Consent Statement: Not applicable.

Data Availability Statement: The raw data supporting the conclusions of this article will be made available by the authors on request.

Conflicts of Interest: The authors declare no conflicts of interest.

References

1. Liu, J.; Hao, X.J.; Zhou, L.; Strangwood, M.; Davis, C.L.; Peyton, A.J. Measurement of microstructure changes in 9Cr-1Mo and 2.25Cr-1Mo steels using an electromagnetic sensor. *Scr. Mater.* **2012**, *66*, 367–370. [CrossRef]
2. Brodecki, A.; Kopec, M.; Kowalewski, Z.L. Monitoring of fatigue damage development in as-received and exploited 10CrMo9-10 power engineering steel supported by Digital Image Correlation. *Int. J. Press. Vessel. Pip.* **2023**, *202*, 104889. [CrossRef]
3. Ławrynowicz, Z. Bainitic reaction and microstructure evolution in two normalized and tempered steels designed for service at elevated temperatures. *Adv. Mater. Sci.* **2017**, *17*, 22–36. [CrossRef]
4. Sirohi, S.; Kumar, S.; Bhanu, V.; Pandey, C.; Gupta, A. Study on the Variation in Mechanical Properties along the Dissimilar Weldments of P22 and P91 Steel. *J. Mater. Eng. Perform.* **2022**, *31*, 2281–2296. [CrossRef]
5. Fadel, A.; Glišić, D.; Radović, N.; Drobnjak, D. Influence of Cr, Mn and Mo Addition on Structure and Properties of V Microalloyed Medium Carbon Steels. *J. Mater. Sci. Technol.* **2012**, *28*, 1053–1058. [CrossRef]
6. Xia, T.; Ma, Y.; Zhang, Y.; Li, J.; Xu, H. Effect of Mo and Cr on the Microstructure and Properties of Low-Alloy Wear-Resistant Steels. *Materials* **2024**, *17*, 2408. [CrossRef] [PubMed]
7. Gwoździk, M.; Motylenko, M.; Rafaja, D. Microstructure changes responsible for the degradation of the 10CrMo9-10 and 13CrMo4-5 steels during long-term operation. *Mater. Res. Express* **2020**, *7*, 016515. [CrossRef]
8. Wang, X.; Li, Y.; Li, H.; Lin, S.; Ren, Y. Effect of long-term aging on the microstructure and mechanical properties of T23 steel weld metal without post-weld heat treatment. *J. Mater. Process. Technol.* **2018**, *252*, 618–627. [CrossRef]
9. Furtado, H.C.; May, I. Le High temperature degradation in power plants and refineries. *Mater. Res.* **2004**, *7*, 103–110. [CrossRef]
10. Watanabe, Y.; Shoji, T. The evaluation of in-service materials degradation of low-alloy steels by the electrochemical method. *Metall. Trans. A* **1991**, *22*, 2097–2106. [CrossRef]
11. Sharma, T.; Bonagani, S.K.; Naveen Kumar, N.; Harish, D.; Mani Krishna, K.V.; Samajdar, I.; Kain, V. Effect of thermal aging on embrittlement of Cr–Mo–V pressure vessel steel. *J. Nucl. Mater.* **2019**, *527*, 151817. [CrossRef]
12. Golański, G.; Pietryka, I.; Jasak, J.; Słania, J.; Urbańczyk, P.; Wieczorek, P. Degradation of Microstructure and Mechanical Properties of 15HM Steel after 420 000 Hours of Service. *Adv. Mater. Sci.* **2014**, *14*, 5–11. [CrossRef]
13. Kopec, M.; Brodecki, A.; Kowalewski, Z.L. Fatigue damage development in 10CrMo9-10 steel for power plant pipes in as-received state and after 280,000 h of exploitation. *Arch. Civ. Mech. Eng.* **2023**, *23*, 98. [CrossRef]
14. Singh, K.; Kamaraj, M. Microstructural degradation in power plant steels and life assessment of power plant components. *Procedia Eng.* **2013**, *55*, 394–401. [CrossRef]
15. Arunkumar, S. Overview of Small Punch Test. *Met. Mater. Int.* **2020**, *26*, 719–738. [CrossRef]
16. Romelczyk-Baishya, B.; Łęczycki, K.; Płocińska, M.; Kulczyk, M.; Molak, R.; Pakieła, Z. The effect of microstructure anisotropy on low temperature fracture of ultrafine-grained iron. *Arch. Civ. Mech. Eng.* **2018**, *18*, 1166–1182. [CrossRef]
17. Foulds, J.; Viswanathan, R. Small Punch Testing for Determining the Material Toughness of Low Alloy Steel Components in Service. *J. Eng. Mater. Technol.* **1994**, *116*, 457–464. [CrossRef]
18. Bruchhausen, M.; Holmström, S.; Simonovski, I.; Austin, T.; Lapetite, J.M.; Ripplinger, S.; de Haan, F. Recent developments in small punch testing: Tensile properties and DBTT. *Theor. Appl. Fract. Mech.* **2016**, *86*, 2–10. [CrossRef]
19. Romelczyk-Baishya, B.; Lumelskyj, D.; Stępniewska, M.; Giżyński, M.; Pakieła, Z. The mechanical properties at room and low temperature of P110 steel characterised by means of small punch test. *Arch. Metall. Mater.* **2019**, *64*, 159–165. [CrossRef]
20. Wang, Z.X.; Shi, H.J.; Lu, J.; Shi, P.; Ma, X.F. Small punch testing for assessing the fracture properties of the reactor vessel steel with different thicknesses. *Nucl. Eng. Des.* **2008**, *238*, 3186–3193. [CrossRef]
21. Alegre, J.M.; Lacalle, R.; Cuesta, I.I.; Álvarez, J.A. Different methodologies to obtain the fracture properties of metallic materials using pre-notched small punch test specimens. *Theor. Appl. Fract. Mech.* **2016**, *86*, 11–18. [CrossRef]
22. Majchrowicz, K.; Romelczyk-Baishya, B.; Wieczorek-Czarnocka, M.; Dobkowska, A.; Raga, K.; Filip, R.; Pakieła, Z. Determination of the fracture toughness of carburized Pyrowear 53 steel for planetary gears by the small punch test method. *Arch. Civ. Mech. Eng.* **2024**, *24*, 177. [CrossRef]
23. Bruchhausen, M.; Holmström, S.; Lapetite, J.M.; Ripplinger, S. On the determination of the ductile to brittle transition temperature from small punch tests on Grade 91 ferritic-martensitic steel. *Int. J. Press. Vessel. Pip.* **2017**, *155*, 27–34. [CrossRef]

24. Stępniewska, M.; Romelczyk-Baishya, B.; Brynk, T.; Giżyński, M.; Pakieła, Z. Influence of low temperature on mechanical properties of carbon steel P110 estimated by means of small punch test. In Proceedings of the 7th International Conference on Fracture Fatigue and Wear, FFW 2018, Ghent, Belgium, 9–10 July 2018; Lecture Notes in Mechanical Engineering; Springer: Singapore, 2019; pp. 151–163.

25. Dobeš, F.; Milička, K. Comparison of conventional and small punch creep tests of mechanically alloyed Al-C-O alloys. *Mater. Charact.* **2008**, *59*, 961–964. [CrossRef]

26. Rouse, J.P.; Cortellino, F.; Sun, W.; Hyde, T.H.; Shingledecker, J. Small punch creep testing: Review on modelling and data interpretation. *Mater. Sci. Technol.* **2013**, *29*, 1328–1345. [CrossRef]

27. *EN 10371:2021*; Metallic Materials—Small Punch Test Method. European Commission: Brussels, Belgium, 2021.

28. Kumar, K.; Pooleery, A.; Madhusoodanan, K.; Singh, R.N.; Chakravartty, J.K.; Shriwastaw, R.S.; Dutta, B.K.; Sinha, R.K. Evaluation of ultimate tensile strength using Miniature Disk Bend Test. *J. Nucl. Mater.* **2015**, *461*, 100–111. [CrossRef]

29. García, T.E.; Rodríguez, C.; Belzunce, F.J.; Suárez, C. Estimation of the mechanical properties of metallic materials by means of the small punch test. *J. Alloys Compd.* **2014**, *582*, 708–717. [CrossRef]

30. Altstadt, E.; Houska, M.; Simonovski, I.; Bruchhausen, M.; Holmström, S.; Lacalle, R. On the estimation of ultimate tensile stress from small punch testing. *Int. J. Mech. Sci.* **2018**, *136*, 85–93. [CrossRef]

31. Altstadt, E.; Ge, H.E.; Kuksenko, V.; Serrano, M.; Houska, M.; Lasan, M.; Bruchhausen, M.; Lapetite, J.M.; Dai, Y. Critical evaluation of the small punch test as a screening procedure for mechanical properties. *J. Nucl. Mater.* **2016**, *472*, 186–195. [CrossRef]

32. Macek, W.; Kopec, M.; Laska, A.; Kowalewski, Z.L. Entire fracture surface topography parameters for fatigue life assessment of 10H2M steel. *J. Constr. Steel Res.* **2024**, *221*, 108890. [CrossRef]

33. Andrés, D.; Dymáček, P. Study of the upper die clamping conditions in the small punch test. *Theor. Appl. Fract. Mech.* **2016**, *86*, 117–123. [CrossRef]

34. Dymáček, P.; Milička, K. Small punch testing and its numerical simulations under constant deflection force conditions. *Strength Mater.* **2008**, *40*, 24–27. [CrossRef]

35. Kaliciak, M.; Uhl, T.; Nowak, M. Statistical analysis and correlation of small punch test. In Proceedings of the SPIE 12488, Health Monitoring of Structural and Biological Systems XVII, Long Beach, CA, USA, 13–16 March 2023; Volume 12488, p. 65.

36. *EN 10028-2:2017*; Flat Products Made of Steels for Pressure Purposes—Part 2: Non-Alloy and Alloy Steels with Specified Elevated Temperature Properties. European Commission: Brussels, Belgium, 2017.

37. *ISO 6892-1:2019*; Metallic Materials—Tensile Testing—Part 1: Method of Test at Room Temperature. ISO: Geneva, Switzerland, 2019.

38. Petzova, J.; Brezina, M.; Kapusnak, M.; Kupca, L. Application of Small Punch Testing Methods for Thermal Ageing Monitoring at Primary Circuit Components in Nuclear Power Plant. In Proceedings of the ASME 2015 Pressure Vessels and Piping Conference, Boston, MA, USA, 19–23 July 2015; p. 45539.

39. Molak, R.M.; Kartal, M.E.; Pakiela, Z.; Kurzydlowski, K.J. The effect of specimen size and surface conditions on the local mechanical properties of 14MoV6 ferritic-pearlitic steel. *Mater. Sci. Eng. A* **2016**, *651*, 810–821. [CrossRef]

40. Sitek, R.; Puchlerska, S.; Nejman, I.; Majchrowicz, K.; Pakieła, Z.; Żaba, K.; Mizera, J. The Impact of Plastic Deformation on the Microstructure and Tensile Strength of Haynes 282 Nickel Superalloy Produced by DMLS and Casting. *Materials* **2022**, *15*, 7545. [CrossRef]

41. Kopec, M.; Brodecki, A.; Kowalewski, Z.L. Quantitative digital image correlation approach for the monitoring of fatigue damage development in 10CrMo9-10 steel in the as-received state and after extended service. *Measurement* **2024**, *234*, 114926. [CrossRef]

42. Kals, R.; Vollertsen, F.; Geiger, M. Scaling effects in sheet metal forming. In Proceedings of the Fourth Conference of Sheet Metal, Enschede, The Netherlands, 1996.

43. Fleury, E.; Ha, J.S. Small punch tests to estimate the mechanical properties of steels for steam power plant: I. Mechanical strength. *Int. J. Press. Vessel. Pip.* **1998**, *75*, 699–706. [CrossRef]

44. Hall, E.O. The Deformation and Ageing of Mild Steel: III Discussion of Results. *Proc. Phys. Soc. Sect. B* **1951**, *64*, 747–753. [CrossRef]

45. Petch, N.J. The cleavage strength of polycrystals. *J. Iron Steel Inst.* **1953**, *174*, 25–28.

46. Zhong, J.; He, Z.; Guan, K.; Jiang, T. Investigation on regression model for the force of small punch test using machine learning. *Int. J. Press. Vessel. Pip.* **2023**, *206*, 105031. [CrossRef]

47. Pan, H.; Peng, J.; Geng, X.; Gao, M.; Miao, X. Prediction of mechanical properties for typical pressure vessel steels by small punch test combined with machine learning. *Int. J. Press. Vessel. Pip.* **2023**, *206*, 105060. [CrossRef]